HHS Public Access

Author manuscript

Oncogene. Author manuscript; available in PMC 2021 April 27.

Published in final edited form as:

Oncogene. 2021 January ; 40(1): 203–214. doi:10.1038/s41388-020-01526-2.

Sox2 is necessary for androgen ablation-induced neuroendocrine differentiation from *Pten* null Sca-1$^+$ prostate luminal cells

Oh-Joon Kwon[1], **Li Zhang**[1], **Deyong Jia**[1], **Li Xin**[1,2,3]

[1]Department of Urology, University of Washington, Seattle, WA 98109

[2]Institute of Stem Cell and Regenerative Medicine, University of Washington, Seattle, WA 98109

Abstract

Prostate adenocarcinoma undergoes neuroendocrine differentiation to acquire resistance toward anti-hormonal therapies. The underlying mechanisms have been investigated extensively, among which Sox2 has been shown to play a critical role. However, genetic evidence in mouse models for prostate cancer to support the crucial role of Sox2 is missing. The adult mouse prostate luminal cells contain both castration-resistant Sox2-expressing Sca-1$^+$ cells and castration-responsive Sca-1$^-$ cells. We show that both types of the luminal cell are susceptible to oncogenic transformation induced by loss of function of the tumor suppressor *Pten*. The tumors derived from the Sca-1$^+$ cells are predisposed to castration resistance and castration-induced neuroendocrine differentiation. Genetic ablation of Sox2 suppresses neuroendocrine differentiation but does not impact the castration resistant property. This study provides direct genetic evidence that Sox2 is necessary for androgen ablation-induced neuroendocrine differentiation of *Pten* null prostate adenocarcinoma, corroborates that the lineage status of the prostate cancer cells is a determinant for its propensity to exhibit lineage plasticity, and supports that the intrinsic features of cell-of-origin for prostate cancers can dictate their clinical behaviors.

Keywords

prostate cancer; castration resistance; neuroendocrine differentiation; Sox2

[3]Corresponding author Li Xin, Ph.D., University of Washington, 850 Republican Street, Seattle, WA 98109, Phone: 206-543-6551, xin18@uw.edu.

Author contributions

Conception and design: L. Xin and O. Kwon
Development of methodology: L. Xin and O. Kwon
Acquisition of data: O. Kwon, L. Zhang, D. Jia
Analysis and interpretation of data: O. Kwon, L. Zhang, D. Jia, L. Xin
Writing, review, and/or revision of the manuscript: L. Xin and O. Kwon
Study supervision: L. Xin

Disclosure of Potential Conflicts of Interest

The authors declare no conflict of interest.

Introduction

Lineage plasticity is defined as a process through which cells transit from one committed developmental pathway to another (1). This mechanism has been employed by various types of tumor cell to adapt to targeted anticancer therapies (2, 3). Prostate adenocarcinoma usually responds to anti-hormonal therapies but almost always recurs and becomes castration resistant. Some castration resistant prostate cancers undergo lineage plasticity, turn on the expression of the markers for the neuroendocrine cells such as Synaptophysin and Chromogranin A, and become an aggressive variant of prostate cancer called neuroendocrine prostate cancer (NEPC) (4–7).

A variety of genetic and epigenetic signaling associated with the development of NEPC have been identified, such as loss of function of tumor suppressors *TP53* and *RB1*, activation of the transcription factor N-Myc and BRN2 and epigenetic regulator EZH2 etc. (8). The cell-fate determining transcription factor Sox2 is functionally implicated in the induction and maintenance of various types of stem and progenitor cells (9). It has been shown as a downstream effector of the NEPC-associated genetic and epigenetic alterations to promote the development of NEPC. For example, AR, TP53 and RB1 suppresses the expression of Sox2 whereas N-Myc, BRN2, EZH2, SRRM4 and LIN28b upregulate its expression (10–14). Sox2 has been suggested to promote NEPC development by regulating *LSD1* (15). However, a critical role of Sox2 during the transition of prostate adenocarcinoma to NEPC has not been demonstrated directly using genetic engineered mouse models for prostate cancer, partly because of a scarcity of mouse models that recapitulates the androgen ablation-induced transition. In this study, we discovered that the prostate adenocarcinoma derived from Pten null Sca-1^{+} mouse prostate luminal cells undergo neuroendocrine differentiation upon androgen deprivation. We demonstrated that Sox2 is necessary for the emergence of androgen-deprivation induced NEPC using this model.

Results

Both the Sca-1^{+} and Sca-1^{-} prostate luminal cells serve as targets for transformation induced by loss of function of *Pten*

Previously, we discovered a distinct Sca-1^{+}Nkx3.1^{-} luminal cell population that resides in the mouse proximal prostatic duct adjacent to the urethra (16, 17). These cells express Sox2, are replicative quiescent, and possess a facultative bipotent differentiation capacity (16–20). We sought to investigate whether they are equally susceptible as the distal luminal cells to transformation induced by loss of function of the tumor suppressor *Pten*, a frequent genetic alteration that occurs in the human prostate cancer. It is easier to distinguish proximal and distal prostatic ducts in the mouse anterior prostate lobe because it is less convoluted than the ventral and dorsolateral lobes. Therefore, although the Sca-1^{+} luminal cells also exist in the proximal ducts of other lobes (16), all results reported in this study were obtained from the anterior lobe unless stated otherwise.

We generated the *K8-CreER^{T2};Pten$^{f/fl}$* compound mice (*K8-Pten*) to achieve tamoxifen-induced ablation of *Pten* in both the proximal and distal luminal cells. One month after tamoxifen treatment, prostatic intraepithelial neoplasia 1/2 (PIN1/2) formed in both

proximal and distal prostatic ducts (N=8, Figure 1A), which progressed to PIN4 lesions and adenocarcinoma 6 months after tamoxifen treatment (N=9, Figure 1A). Co-immunostaining of pAKT and K8 demonstrates successful deletion of Pten in both proximal and distal luminal cells (Figure 1B). PIN lesions derived from both regions are composed of mostly luminal cells that express AR and K8 surrounded by Krt5 or Krt14 positive basal cells (Figure 1C). The expression levels of AR in the two groups are comparable but Nkx3.1 is undetectable in the PIN lesions at the proximal ducts (dot plots, Figure 1C). Interestingly, Sox2 is turned on in the luminal cells in the PIN lesions at distal ducts but the expression level is substantially lower than the endogenous level of Sox2 in the Sca-1$^+$ cells at the proximal duct (Figure 1D). Finally, despite the quiescent property of the proximal luminal cells, the proliferative indices of the tumor cells in the distal and proximal regions are comparable (Figures 1E–F). These results demonstrate that the Sca-1$^+$ and Sca-1$^-$ luminal cells are both susceptible to transformation induced by loss of function of Pten.

Prostate cancer originating from the Sca-1$^+$ luminal cells are castration resistant

The Sca-1$^+$ luminal cells do not rely on androgen for their survival (17, 18, 20). To examine whether tumors derived from the Sca-1$^+$ luminal cells inherit the castration resistant property of their cells of origin, we castrated *K8-Pten* mice at 3 months after tamoxifen induction (Figure 2A). Figure 2B shows that the tumor cells in both proximal and distal ducts display a higher nuclear/cytoplasm ratio, which is a typical result of androgen ablation. Immunostaining shows a low to undetectable level of cytoplasmic AR staining after castration, corroborating successful androgen deprivation (Figure 2C). Immunostaining of Ki67 shows that the proliferative indices of the tumors in the proximal and distal regions were reduced by 2.39- and 2.68-fold after castration, respectively, but remained comparable to each other (Figures 1F and 2D). Immunostaining of cleaved caspase 3 (CC3) shows that the apoptotic index of the tumor cells in both regions increased significantly after castration (5.79-fold at proximal region and 41.1-fold at distal region), and the apoptotic index at the distal region is 3.76-fold higher than that in the proximal duct (Figure 2E).

During prostate cancer development, tumor cells may migrate inside the intraductal space, making their origin hard to define. We used an alternative experimental design (Figure 3A) to ensure that the tumors subjected to the study definitively originated from proximal and distal luminal cells, respectively, and used this complementary approach to further corroborate the differential response of the tumors in different regions to androgen ablation. In this approach, proximal and distal prostate tissues were separated and transplanted separately before prostate cancer developed. This excluded the possibility that tumors originating from different regions may migrate and mix. Briefly, we dissected distal and proximal tissue chunks of the same weight from *K8-Pten* mice shortly (one week) after tamoxifen treatment and transplanted them under the kidney capsules of immunodeficient male mice, separately (Figure 3A). Three months after the transplantation, host mice were either castrated or underwent mock surgery and the transplanted tissues were incubated for another 3 months in the hosts. Figures 3B–C show that the average sizes/weight of the tumors outgrown from the proximal and distal tissue chunks in intact hosts are comparable, corroborating that they are equally susceptible to transformation. The weight of the distal duct-derived tumors in castrated host is approximately half of that of the tumors grown in

intact host, confirming their castration sensitive feature. In contrast, the weight of the tumors derived from the proximal tissues in intact and castrated hosts is comparable, corroborating their castration resistant property.

H&E staining and immunostaining of lineage markers show that there was not much difference between the tumors in respective anatomic regions before and after androgen deprivation (Figures 3D–E). The proliferative indices of the tumor cells originating from distal and proximal regions were significantly decreased by 43% and 30%, respectively, after castration but were not significantly different from each other (Figure 3F and Supplementary Figure 1A). The apoptotic indices of the tumors increased in the castration group, but the apoptotic index of the tumors derived from the distal luminal cells was 2.3-fold higher than that of the tumors from the proximal luminal cells after castration (Figure 3G and Supplementary Figure 1B). AR displays a diffusive cytoplasmic staining in the tumors in the castrated hosts versus a clear nuclear staining in the intact groups, confirming the successful androgen deprivation (Supplementary Figure 1C). Another interesting observation in the tumors in intact mice is that there are more $AR^{-}Krt8^{+}$ tumor cells in the proximal duct-originating tumors than in the distal duct-originating tumors (Figure 3H and Supplementary Figure 1C). Collectively, these results demonstrate that although the proximal and distal luminal cells are equally susceptible to transformation induced by loss of function of Pten, the tumors derived from the proximal luminal cells are relatively resistant to androgen deprivation.

Prostate cancer in proximal prostate of *K8-Pten* mice undergoes neuroendocrine differentiation in response to androgen deprivation

The neuroendocrine (NE) cells that express Chromogranin A (Chga) are very rare among the PIN lesions in intact *K8-Pten* mice (Figure 4A) especially in the distal PIN lesions. This pattern is consistent with the observation that more NE cells are present in the proximal prostatic ducts than in distal ducts in adult wild type mice (Supplementary Figure 2A, p=0.0041). 77.8% of the $Chga^{+}$ cells are presented as single cells and the rest in clusters of 3–5 cells at the proximal ducts of intact *K8-Pten* mice. In contrast, almost all $Chga^{+}$ cells are presented as single cells in the distal ducts of *K8-Pten* mice (Figure 4B). Interestingly, the frequency of the NE cells in proximal duct prostate cancer increased after castration (Figure 4B, p=0.0004 by Mann-Whitney U test, and Supplementary Figure 2B). In addition, about half of the NE cells are now presented in clusters of 3–5 cells and the rest in clusters with more than 10 cells. The expansion of NE cells in proximal duct-originating tumors in response to androgen deprivation was also corroborated in the transplantation experiments shown in Figure. 3A (Figure 4C, p=0.0188 by Mann-Whitney U test).

Figure. 4D shows that pAKT is upregulated and Pten is absent in these NE cells. Two possible mechanisms can account for the expansion of NE cells. First, some prostate adenocarcinoma can undergo NE differentiation upon androgen deprivation (5) and upregulation of Sox2 contributes to NE differentiation (10). Therefore, it is possible that the $Sox2^{high}$ cancer cells in proximal prostate are predisposed to NE differentiation, thereby leading to an expansion of NE-like cells after androgen deprivation. Alternatively, the $pAKT^{+}$ NE cells may originate from the endogenous NE cells directly because of androgen

deprivation and Pten ablation. Since there is no expansion of NE cells in both distal and proximal ducts in castrated WT mice (Supplementary Figure 2C), it is unlikely that castration per se can stimulate the proliferation of NE cells. Using the *K8-eYFP* model we confirmed that some NE cells were labeled with eYFP (Supplementary Figure 2D), suggesting that *Pten* could be disrupted in the NE cells in the *K8-Pten* model, too. However, we only observed the expansion of NE cells in the proximal prostate cancer tissues after androgen ablation in both the de novo (Figures 4A and 4B) and transplantation (Figure 4C) models. Therefore, it is also unlikely that disrupting Pten in NE cells promotes their proliferation upon androgen deprivation. Finally, very few NE cells proliferated actively (2 out of 906 cells counted, Figure 4E), further supporting that they may not emerge through self-duplication of NE cells. Co-immunostaining of Syp and CC3 also shows that the Syp^{+} cells did not undergo apoptosis upon androgen deprivation (Supplementary Fig. 3). Collectively, these results support that the expanded NE cells in the proximal ducts in castrated mice are most likely transdifferentiated from the $Sox2^{high}$ prostate cancer cells and imply that that the $Sox2^{high}$ prostate cancer cells are predisposed to NE differentiation in response to androgen deprivation.

Sox2 is necessary for the androgen-deprivation induced neuroendocrine differentiation

We recently demonstrated that Sox2 is not essential for the maintenance of the prostate epithelial tissues using a *K8-CreER^{T2};Sox2$^{fl/fl}$* compound mouse model (17). Sox2 is not only highly expressed endogenously in the proximal luminal epithelial cells but is also upregulated in the luminal cells in distal ducts in the *K8-Pten* model (Figure 1D). We investigated whether Sox2 is essential for the initiation and progression of the cancer in proximal and distal ducts in the *K8-Pten* model. We generated a cohort of *K8-CreER^{T2};Pten$^{fl/fl}$;Sox2$^{fl/fl}$* (*K8-Pten-Sox2*) and *K8-Pten* mice. Eight-week-old mice were treated with tamoxifen and aged. Figure. 5A shows that there is no significant difference in prostate weight between the two groups even 6 months after tamoxifen treatment. The PIN lesions in the two groups are histologically indistinguishable (Figure 5B, intact). Immunostaining of Sox2 and pAKT1 confirms that Sox2 and Pten were successfully deleted (Figure 5C, intact). This result indicates that Sox2 is dispensable for the initiation of PIN lesions in both proximal and distal ducts.

To determine whether Sox2 plays a role in proliferation and survival of tumor cells after androgen deprivation, we castrated *K8-Pten-Sox2* and *K8-Pten* mice 3 months after they were treated with tamoxifen and determined how the prostate tissues responded. Immunostaining of AR and Nkx3.1 confirms successful disruption of AR and its activity (Supplementary Figures 4A and 4B). The PIN lesions in both groups responded to androgen deprivation similarly (Figures 5A–B, castration). Consistent with data shown in Figures 2D and 2E, the proliferative indices at the proximal and distal PIN lesions in intact *K8-Pten* mice were comparable and were reduced to a similar extent upon androgen deprivation (Figure 5D and Supplementary Figure 4C), and the apoptotic index in the distal PIN lesions in *K8-Pten* mice was higher than that in the proximal PIN lesions upon androgen deprivation (Figure 5E and Supplementary Figure 4C). The proliferative and apoptotic indices of the PIN lesions at different anatomic locations of the *K8-Pten-Sox2* mice as well as their changes upon androgen deprivation were not significantly different from those of the *K8-*

Pten mice, respectively (Figures 5D–E, and Supplementary Figure 4C). These results support that Sox2 is not critical for the proliferation and survival of the *Pten* null tumor cells. To further corroborate the dispensability of Sox2 in proliferation and survival, we performed a similar transplantation experiment as described in Figure 3A and reached the same conclusion (Supplementary Figures 5A–B).

The frequency and distribution pattern of the $Chga^+$ or Syp^+ neuroendocrine cells are similar in intact *K8-Pten* and *K8-Pten-Sox2* mice (Figure 6A–B, intact). As shown previously in Figure 4B, castration drove the expansion of the cells expressing the NE cell markers (Syp and Chga) in the proximal PIN lesions in the *K8-Pten* mice (p=0.00676, Mann-Whitney U test). In contrast, although there is also a trend with increased neuroendocrine cell colonies in the *K8-Pten-Sox2* mice after androgen deprivation, the change is not statistically significant (p=0.0642, Mann-Whitney U test) (Figures 6A–B, castration). Similarly, in the transplantation experiment, we also confirmed that the average size of the NE cell colonies was significantly increased in the transplanted proximal PIN lesions of the *K8-Pten* mice (p=0.0222, Mann-Whitney U test) but not in those of the *K8-Pten-Sox2* mice (p=0.115, Mann-Whitney U test) after androgen deprivation (Figures 6C–D). These results show that Sox2 is necessary for the NE differentiation of the *Pten* null tumor cells. Of note, the insignificant trend with increased NE colonies in the *K8-Pten-Sox2* mice after androgen deprivation is either because of an incomplete disruption of Sox2 or implies the contribution of other factors in castration-induced NE differentiation.

The cells underwent neuroendocrine differentiation only constituted a small portion of the tumor cells that survived castration. In addition, ablating Sox2 attenuated NE differentiation but did not affect castration resistance. Therefore, it is unlikely that the NE differentiation is the major mechanism of the castration resistance for the proximal prostate tumor cells in the *Pten* null model. The proximal prostate tumor cells arose from the $Sca\text{-}1^+$ luminal cells that do not rely on the androgen signaling for their survival (17). Therefore, it is more likely that these tumor cells inherit an intrinsic capacity for castration resistance from their cell-of-origin.

Discussion

Prostate cancers respond to anti-androgen therapies differently, with some developing resistance faster via transition to NEPC. The molecular mechanisms underlying the heterogeneous responses remains incompletely understood. The cells-of-origin for cancer is generally defined as the cells within a tissue from which cancer originates (21). One interesting theory is that the identity of the cell-of-origin for cancers can determine their clinical behavior (22, 23). Our study shows that both the $Sca\text{-}1^+$ and $Sca\text{-}1^-$ luminal cells can serve as cells-of-origin for transformation, which is consistent with a recent study (24). One unique finding of ours is that the prostate adenocarcinoma derived from the $Sca\text{-}1^+$ luminal cells are predisposed to neuroendocrine differentiation upon androgen ablation. We and other have shown that the human prostate luminal cells expressing a high level of TACSTD2 display similar molecular and phenotypic features with the mouse $Sca\text{-}1^+$ luminal cells (17, 25). Therefore, one intuitive implication from our study is that some human prostate cancers were inclined to undergo neuroendocrine differentiation when challenged

by androgen deprivation probably because they arose from the TACSTD2^{+} luminal cells. This hypothesis is supported by a recent study showing that high expression of TACSTD2 was associated with biochemical recurrence (26). In addition, our recent study demonstrated directly that, when transduced with activated AKT1 and c-Myc, the TACSTD2^{high} human prostate luminal cells possess a higher potential to undergo lineage plasticity and generate organoids containing distinct clinically relevant prostate tumor cell populations than the TACSTD2^{low} luminal cells (27). Prostate ductal adenocarcinoma (PDA) is rare but is the second common histological variant of prostatic carcinoma (28, 29). It is an aggressive subtype of prostate cancer with higher risk of disease progression. PDAs predominantly locate in the periurethral zone of prostate and some of PDAs express KRT7 (30, 31). Interestingly, our current and recent studies show that the mouse Sca-1^{+} and human TACSTD2^{high} luminal cells are both preferentially enriched in the periurethral zones and specifically express Krt7 (17). We showed that tumors derived from these two types of luminal cell are castration resistant and display a higher propensity for lineage plasticity. Therefore, it is tempting to hypothesize that these cells may serve as the cell-of-origin for PDAs.

Nevertheless, this cell-of-origin hypothesis should not exclusively account for the heterogenous response of prostate cancers to therapies, especially the intra-patient heterogeneity of response. An alternative implication from our study is that the cellular state of cancer cells determines their potential to exhibit lineage plasticity. This has been shown in previous studies that the genetic and epigenetic alterations associated with NEPC often rewire the global transcriptional profiles of the cancer cells, which either facilitates or directly drives the transition of cellular identity (8). *SOX2* has been shown as an AR-repressed gene (32). The dosage of Sox2 is also important for cell fate determination (33). Androgen deprivation may upregulate SOX2 expression to different levels among tumor cells, thereby affecting their potential to undergo NE differentiation. Since SOX2 is highly expressed in the human prostate cancer cell lines that do not display an NE phenotype (34), we reason that SOX2 more likely facilitates NE differentiation rather than directly driving NE differentiation.

Currently, there are only a few mouse models for *de novo* or castration induced NEPC. Most of the models incorporated genetic alterations associated with human NEPC, such as knockout or loss of function of *Trp53* and *Rb1* and increased activity of N-Myc (6, 13, 35–37). The prostate specific *Pten* null mice was widely used as a model for prostate adenocarcinoma but not NEPC (38–40). We were able to discover the rare NEPC feature induced by castration in this genetic context for two reasons. First, the castration induced NEPC only occurs in the proximal region which may be overlooked in previous studies; second, the Sca-1^{+} luminal cells do not express *Nkx3.1* and *Probasin*, therefore cannot be targeted in the models using the *Pbsn-Cre* and *Nkx3.1-CreER^{T2}* lines (38, 41). The Sca-1^{+} luminal cells highly express Sox2, which confers them a higher potential for being reprogramed to neuroendocrine lineages. Interesting, a previous study has suggested that a SoxC member Sox11 may also play a role in the emergence of NEPC in a mouse model for prostate cancer with dual knockout of *Pten* and *Trp53* (6).

Besides the intrinsic property of the Sca-1^+ luminal cells, their tissue microenvironment may also contribute to the formation of NEPC. We showed that the stromal cells in the proximal prostate where the Sca-1^+ luminal cells reside express high levels of various Wnt ligands (42). The turnover rate of the epithelial cells in the proximal regions is extremely low under physiological conditions, partly because of the activation of the epithelial cell intrinsic non-canonical Wnt signaling. But in the context of oncogenic transformation, the Wnt ligands secreted by the stromal cells may activate Wnt signaling in the Pten null tumor cells to promote NE differentiation, which has been reported previously (43). Interestingly, the tumor cells that express the NE cell markers are mostly mitotic inert in our model, which is consistent with an observation made in the prostate cancer mouse model induced by loss of function of Pten and Tp53 (6). This may be partly accounted for by previous studies showing that SOX2 confers tumor cell dormancy in certain genetic contexts (33). Future studies will be performed to further investigate the molecular mechanisms regulating the emergence and expansion of the NEPC in mouse models.

Materials and Methods

Mice

The C57Bl/6, *Gt(ROSA)26Sor*$^{tm1(EYFP)Cos/J}$, *Sox2*$^{tm1.1Lan/}$J and *Pten*$^{tm1Hwu/}$J mice were purchased from The Jackson Laboratory (Bar Harbor, ME). The SCID/Beige mice were purchased from Charles River (Wilmington, MA). The *K8-CreER*^{T2} mice were generated by our group previously (Zhang et al, 2012). All mice are on C57Bl/6 background unless stated otherwise. Mice were genotyped by polymerase chain reaction using mouse genomic DNA from tail biopsy specimens. The sequences of genotyping primers are listed in Supplementary Table 1. PCR products were separated electophoretically on 1% agarose gels and visualized via ethidium bromide under UV light.

Tamoxifen treatment and androgen deprivation

Tamoxifen (Sigma-Aldrich, St. Louis, MO) was dissolved in corn oil and administrated i.p. into experimental mice at the specified age (*K8-eYFP*: 2mg/40g/day for 4 consecutive days, *K8-Pten,* and *K8-Pten-Sox2*: 7mg/40g/day for 4 consecutive days). For androgen deprivation, experimental mice were castrated using standard techniques as described previously (Kwon et al., 2016)

Prostate tissue transplantation under kidney capsule

The proximal and distal prostatic tissue chunks (2–3 mm) from anterior lobes of tamoxifen-treated *K8-Pten* or *K8-Pten-Sox2* mice were weighed and grafted under the renal capsules of SCID/Beige mice as described previously (44). Three months later, host mice were either castrated or underwent mock surgery. Tissues were collected after another 3-month incubation.

Histology and Immunostaining

Murine prostate tissues were fixed by 10% buffered formalin and paraffin embedded. H&E staining and immunofluorescence staining were performed using standard protocols on 5-μm paraffin sections. Slides were incubated with 5% normal goat serum (Vector Labs,

Burlingame, CA) and with primary antibodies diluted in 3% normal goat serum overnight at 4°C. Information for primary antibodies is listed in Supplementary Table 2. Slides were then incubated with secondary antibodies (diluted 1:500 in 0.05% tween 20 in PBS) labeled with Alexa Fluor 488, 568, 594, or 633 (Invitrogen/Molecular Probes, Eugene, OR). Sections were counterstained with NucBlue™ Fixed Cell ReadyProbes™ Reagent (Thermo Fisher). Immuno-fluorescence staining was imaged using Leica DM4B fluorescent microscope or LeicaSP8 confocal microscope (Leica Microsystems, Wetzlar, Germany). All representative images were quantified by the Image J software.

Statistics

All experiments were performed using 4–10 mice in independent experiments. Data are presented as mean ± SD or mean ± SEM. Student's t test or Mann-Whitney U test were used to determine significance between groups. All p values reported were two-sided unless otherwise noted. For all statistical tests, the 0.05 level of confidence was accepted for statistical significance.

Study approval

All the mice used in this study received humane care in compliance with the principles stated in the Guide for the Care and Use of Laboratory Animals, NIH Publication, 1996 edition, and the protocols were approved by the Institutional Animal Care Committee at the University of Washington.

Supplementary Material

Refer to Web version on PubMed Central for supplementary material.

Acknowledgements

This work is supported by R01CA190378 (L.X.).

References

1. Quintanal-Villalonga A, Chan JM, Yu HA, Pe'er D, Sawyers CL, Sen T, et al. Lineage plasticity in cancer: a shared pathway of therapeutic resistance. Nature reviews Clinical oncology. 2020;17(6):360–71. Epub 2020/03/11.
2. Sequist LV, Waltman BA, Dias-Santagata D, Digumarthy S, Turke AB, Fidias P, et al. Genotypic and histological evolution of lung cancers acquiring resistance to EGFR inhibitors. Science translational medicine. 2011;3(75):75ra26. Epub 2011/03/25.
3. Konieczkowski DJ, Johannessen CM, Abudayyeh O, Kim JW, Cooper ZA, Piris A, et al. A melanoma cell state distinction influences sensitivity to MAPK pathway inhibitors. Cancer discovery. 2014;4(7):816–27. Epub 2014/04/29. [PubMed: 24771846]
4. Labrecque MP, Coleman IM, Brown LG, True LD, Kollath L, Lakely B, et al. Molecular profiling stratifies diverse phenotypes of treatment-refractory metastatic castration-resistant prostate cancer. The Journal of clinical investigation. 2019;130:4492–505. Epub 2019/07/31.
5. Davies AH, Beltran H, Zoubeidi A. Cellular plasticity and the neuroendocrine phenotype in prostate cancer. Nature reviews Urology. 2018;15(5):271–86. Epub 2018/02/21. [PubMed: 29460922]
6. Zou M, Toivanen R, Mitrofanova A, Floch N, Hayati S, Sun Y, et al. Transdifferentiation as a Mechanism of Treatment Resistance in a Mouse Model of Castration-Resistant Prostate Cancer. Cancer discovery. 2017;7(7):736–49. Epub 2017/04/16. [PubMed: 28411207]

7. Lin D, Wyatt AW, Xue H, Wang Y, Dong X, Haegert A, et al. High fidelity patient-derived xenografts for accelerating prostate cancer discovery and drug development. Cancer Res. 2014;74(4):1272–83. Epub 2013/12/21. [PubMed: 24356420]
8. Beltran H, Hruszkewycz A, Scher HI, Hildesheim J, Isaacs J, Yu EY, et al. The Role of Lineage Plasticity in Prostate Cancer Therapy Resistance. Clin Cancer Res. 2019;25(23):6916–24. Epub 2019/08/01. [PubMed: 31363002]
9. Schaefer T, Lengerke C. SOX2 protein biochemistry in stemness, reprogramming, and cancer: the PI3K/AKT/SOX2 axis and beyond. Oncogene. 2020;39(2):278–92. Epub 2019/09/04. [PubMed: 31477842]
10. Mu P, Zhang Z, Benelli M, Karthaus WR, Hoover E, Chen CC, et al. SOX2 promotes lineage plasticity and antiandrogen resistance in TP53- and RB1-deficient prostate cancer. Science. 2017;355(6320):84–8. Epub 2017/01/07. [PubMed: 28059768]
11. Lee AR, Gan Y, Tang Y, Dong X. A novel mechanism of SRRM4 in promoting neuroendocrine prostate cancer development via a pluripotency gene network. EBioMedicine. 2018;35:167–77. Epub 2018/08/14. [PubMed: 30100395]
12. Bishop JL, Thaper D, Vahid S, Davies A, Ketola K, Kuruma H, et al. The Master Neural Transcription Factor BRN2 Is an Androgen Receptor-Suppressed Driver of Neuroendocrine Differentiation in Prostate Cancer. Cancer discovery. 2017;7(1):54–71. Epub 2016/10/28. [PubMed: 27784708]
13. Berger A, Brady NJ, Bareja R, Robinson B, Conteduca V, Augello MA, et al. N-Myc-mediated epigenetic reprogramming drives lineage plasticity in advanced prostate cancer. The Journal of clinical investigation. 2019;130:3924–40. Epub 2019/07/02.
14. Lovnicki J, Gan Y, Feng T, Li Y, Xie N, Ho CH, et al. LIN28B promotes the development of neuroendocrine prostate cancer. The Journal of clinical investigation. 2020. Epub 2020/07/08.
15. Li H, Wang L, Li Z, Geng X, Li M, Tang Q, et al. SOX2 has dual functions as a regulator in the progression of neuroendocrine prostate cancer. Laboratory investigation; a journal of technical methods and pathology. 2020;100(4):570–82. Epub 2019/11/28. [PubMed: 31772313]
16. Kwon OJ, Zhang L, Xin L. Stem Cell Antigen-1 Identifies a Distinct Androgen-Independent Murine Prostatic Luminal Cell Lineage with Bipotent Potential. Stem Cells. 2016;34(1):191–202. Epub 2015/09/30. [PubMed: 26418304]
17. Kwon OJ, Choi JM, Zhang L, Jia D, Li Z, Zhang Y, et al. The Sca-1(+) and Sca-1(−) mouse prostatic luminal cell lineages are independently sustained. Stem Cells. 2020. Epub 2020/07/07.
18. Tsujimura A, Koikawa Y, Salm S, Takao T, Coetzee S, Moscatelli D, et al. Proximal location of mouse prostate epithelial stem cells: a model of prostatic homeostasis. J Cell Biol. 2002;157(7):1257–65. [PubMed: 12082083]
19. Zhang D, Jeter C, Gong S, Tracz A, Lu Y, Shen J, et al. Histone 2B-GFP Label-Retaining Prostate Luminal Cells Possess Progenitor Cell Properties and Are Intrinsically Resistant to Castration. Stem cell reports. 2018;10(1):228–42. Epub 2017/12/26. [PubMed: 29276153]
20. McAuley E, Moline D, VanOpstall C, Lamperis S, Brown R, Vander Griend DJ. Sox2 Expression Marks Castration-Resistant Progenitor Cells in the Adult Murine Prostate. Stem Cells. 2019;37(5):690–700. Epub 2019/02/06. [PubMed: 30720908]
21. Xin L. Cells of Origin for Prostate Cancer. Advances in experimental medicine and biology. 2019;1210:67–86. Epub 2020/01/05. [PubMed: 31900905]
22. Latil M, Nassar D, Beck B, Boumahdi S, Wang L, Brisebarre A, et al. Cell-Type-Specific Chromatin States Differentially Prime Squamous Cell Carcinoma Tumor-Initiating Cells for Epithelial to Mesenchymal Transition. Cell stem cell. 2017;20(2):191–204 e5. Epub 2016/11/28. [PubMed: 27889319]
23. Gupta PB, Kuperwasser C, Brunet JP, Ramaswamy S, Kuo WL, Gray JW, et al. The melanocyte differentiation program predisposes to metastasis after neoplastic transformation. Nature genetics. 2005;37(10):1047–54. Epub 2005/09/06. [PubMed: 16142232]
24. Guo W, Li L, He J, Liu Z, Han M, Li F, et al. Single-cell transcriptomics identifies a distinct luminal progenitor cell type in distal prostate invagination tips. Nature genetics. 2020;52(9):908–18. Epub 2020/08/19. [PubMed: 32807988]

25. Crowell PD, Fox JJ, Hashimoto T, Diaz JA, Navarro HI, Henry GH, et al. Expansion of Luminal Progenitor Cells in the Aging Mouse and Human Prostate. Cell reports. 2019;28(6):1499–510 e6. Epub 2019/08/08. [PubMed: 31390564]
26. Hsu EC, Rice MA, Bermudez A, Marques FJG, Aslan M, Liu S, et al. Trop2 is a driver of metastatic prostate cancer with neuroendocrine phenotype via PARP1. Proc Natl Acad Sci U S A. 2020;117(4):2032–42. Epub 2020/01/15. [PubMed: 31932422]
27. Kwon OJ, Zhang L, Jia D, Zhou Z, Li Z, Haffner M, et al. De novo induction of lineage plasticity from human prostate luminal epithelial cells by activated AKT1 and c-Myc. Oncogene. 2020. Epub 2020/10/04.
28. Liu T, Wang Y, Zhou R, Li H, Cheng H, Zhang J. The update of prostatic ductal adenocarcinoma. Chinese journal of cancer research = Chung-kuo yen cheng yen chiu. 2016;28(1):50–7. Epub 2016/04/05. [PubMed: 27041926]
29. Fine SW. Variants and unusual patterns of prostate cancer: clinicopathologic and differential diagnostic considerations. Advances in anatomic pathology. 2012;19(4):204–16. Epub 2012/06/14. [PubMed: 22692283]
30. Lee TK, Miller JS, Epstein JI. Rare histological patterns of prostatic ductal adenocarcinoma. Pathology. 2010;42(4):319–24. Epub 2010/05/05. [PubMed: 20438402]
31. Goldstein NS. Immunophenotypic characterization of 225 prostate adenocarcinomas with intermediate or high Gleason scores. American journal of clinical pathology. 2002;117(3):471–7. Epub 2002/03/13. [PubMed: 11888088]
32. Kregel S, Kiriluk KJ, Rosen AM, Cai Y, Reyes EE, Otto KB, et al. Sox2 is an androgen receptor-repressed gene that promotes castration-resistant prostate cancer. PLoS One. 2013;8(1):e53701. Epub 2013/01/18.
33. Metz EP, Rizzino A. Sox2 dosage: A critical determinant in the functions of Sox2 in both normal and tumor cells. Journal of cellular physiology. 2019;234(11):19298–306. Epub 2019/07/28. [PubMed: 31344986]
34. Yu X, Cates JM, Morrissey C, You C, Grabowska MM, Zhang J, et al. SOX2 expression in the developing, adult, as well as, diseased prostate. Prostate cancer and prostatic diseases. 2014;17(4):301–9. Epub 2014/08/06. [PubMed: 25091041]
35. Ku SY, Rosario S, Wang Y, Mu P, Seshadri M, Goodrich ZW, et al. Rb1 and Trp53 cooperate to suppress prostate cancer lineage plasticity, metastasis, and antiandrogen resistance. Science. 2017;355(6320):78–83. Epub 2017/01/07. [PubMed: 28059767]
36. Masumori N, Thomas TZ, Chaurand P, Case T, Paul M, Kasper S, et al. A probasin-large T antigen transgenic mouse line develops prostate adenocarcinoma and neuroendocrine carcinoma with metastatic potential. Cancer Res. 2001;61(5):2239–49. [PubMed: 11280793]
37. Zhou Z, Flesken-Nikitin A, Nikitin AY. Prostate cancer associated with p53 and Rb deficiency arises from the stem/progenitor cell-enriched proximal region of prostatic ducts. Cancer Res. 2007;67(12):5683–90. Epub 2007/06/08. [PubMed: 17553900]
38. Wang S, Gao J, Lei Q, Rozengurt N, Pritchard C, Jiao J, et al. Prostate-specific deletion of the murine Pten tumor suppressor gene leads to metastatic prostate cancer. Cancer Cell. 2003;4(3):209–21. [PubMed: 14522255]
39. Ma X, Ziel-van der Made AC, Autar B, van der Korput HA, Vermeij M, van Duijn P, et al. Targeted biallelic inactivation of Pten in the mouse prostate leads to prostate cancer accompanied by increased epithelial cell proliferation but not by reduced apoptosis. Cancer Res. 2005;65(13):5730–9. [PubMed: 15994948]
40. Backman SA, Ghazarian D, So K, Sanchez O, Wagner KU, Hennighausen L, et al. Early onset of neoplasia in the prostate and skin of mice with tissue-specific deletion of Pten. Proc Natl Acad Sci U S A. 2004;101(6):1725–30. Epub 2004/01/30. [PubMed: 14747659]
41. Wang ZA, Mitrofanova A, Bergren SK, Abate-Shen C, Cardiff RD, Califano A, et al. Lineage analysis of basal epithelial cells reveals their unexpected plasticity and supports a cell-of-origin model for prostate cancer heterogeneity. Nature cell biology. 2013;15(3):274–83. Epub 2013/02/26. [PubMed: 23434823]

42. Wei X, Zhang L, Zhou Z, Kwon OJ, Zhang Y, Nguyen H, et al. Spatially Restricted Stromal Wnt Signaling Restrains Prostate Epithelial Progenitor Growth through Direct and Indirect Mechanisms. Cell stem cell. 2019;24(5):753–68 e6. Epub 2019/04/16. [PubMed: 30982770]

43. Yu X, Wang Y, DeGraff DJ, Wills ML, Matusik RJ. Wnt/beta-catenin activation promotes prostate tumor progression in a mouse model. Oncogene. 2011;30(16):1868–79. Epub 2010/12/15. [PubMed: 21151173]

44. Kwon OJ, Zhang L, Wang J, Su Q, Feng Q, Zhang XH, et al. Notch promotes tumor metastasis in a prostate-specific Pten-null mouse model. The Journal of clinical investigation. 2016;126(7):2626–41. Epub 2016/06/14. [PubMed: 27294523]

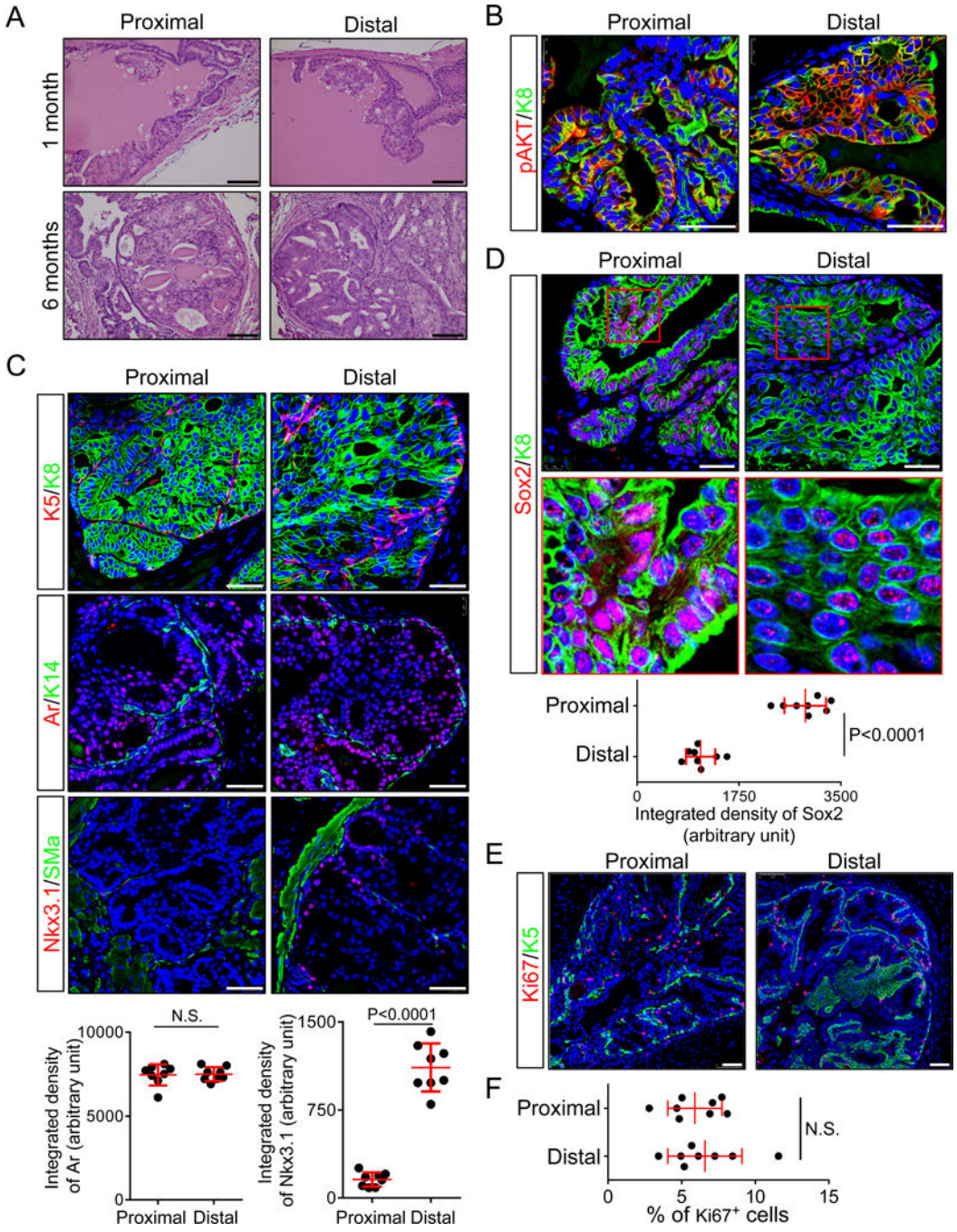

Figure 1. Both Sca-1^{+} and Sca-1^{-} luminal cells can serve as targets for transformation induced by *Pten* loss.

(A) H&E staining of proximal and distal anterior prostate of *K8-Pten* mice at 1 and 6 months after tamoxifen treatment (N=8 and 9, respectively). Scale bars:100 μm. (B-C) Co-immunostaining of pAKT/K8 (B), K5/K8 (C, upper), Ar/K14 (C, middle), and Nkx3.1/ Smooth muscle actin (SMa) (C, lower) in proximal and distal prostates of *K8-Pten* mice 6 months after tamoxifen treatment. Scale bars:50 μm. Dot plots show integrated density of staining of Ar (left) and Nkx3.1 (right) (N=8, each dot represents average value from 3 representative images from each mouse). (D) Co-immunostaining of Sox2/K8 in proximal

and distal prostates of *K8-Pten* mice 6 months after tamoxifen treatment. Scale bars:50 μm. Dot plot shows integrated density of staining of Sox2 (N=8, each dot represents average value from 3 representative images from each mouse). (E) Co-immunostaining of Ki67/K5 in proximal and distal prostates of *K8-Pten* mice 6 months after tamoxifen treatment. Scale bars:50 μm. (F) Dot plot shows means ± SD of percentage of $Ki67^+$ cells in proximal and distal prostates of *K8-Pten* mice 6 months after tamoxifen treatment (N=8, each dot represents average value from 6 representative images of individual mouse). N.S.: no significance.

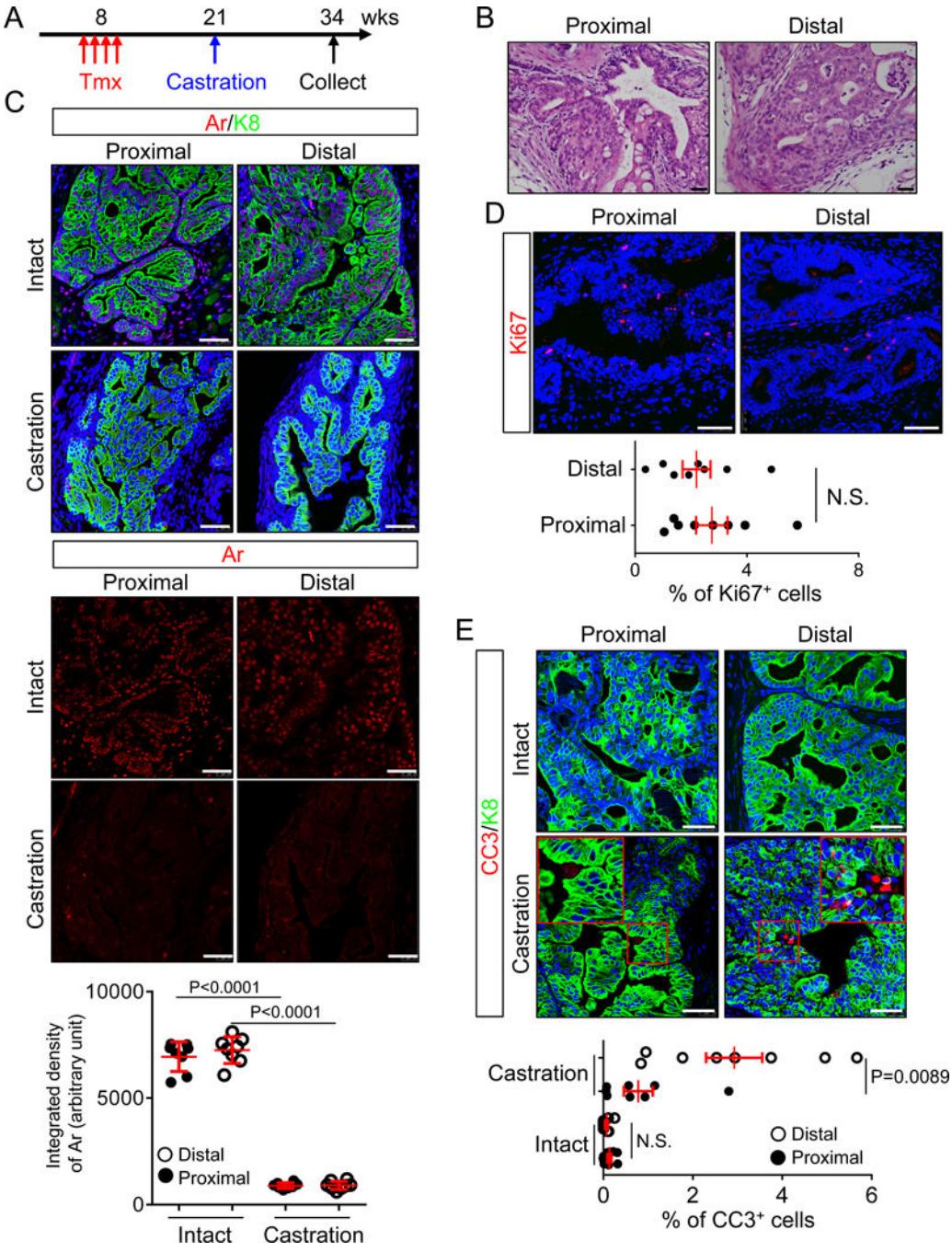

Figure 2. Prostate cancer derived from Sca-1^{+} luminal cells displays castration-resistance.

(A) Schematic illustration of experimental design. Tmx: tamoxifen. (B) H&E staining of proximal and distal anterior prostates of castrated *K8-Pten* mice. Scale bar: 25 μm. (C) Co-immunostaining of Ar/K8 (upper panels) in proximal and distal prostates of intact and castrated *K8-Pten* mice. Lower panels show Ar staining only. Scale bar: 50 μm. Dot plot shows integrated density of Ar staining (N=8, each dot represents average value from 3 representative images from each mouse). (D-E) Immunostaining of Ki67 (E) and cleaved caspase 3 (CC3) (F) in proximal and distal regions of androgen depleted *K8-Pten* mice.

Scale bars:50 μm. Dot plots show means ± SD of percentage of positively stained cells (N=8, each dot shows average value from 6 representative images of individual mice). N.S.; no significance.

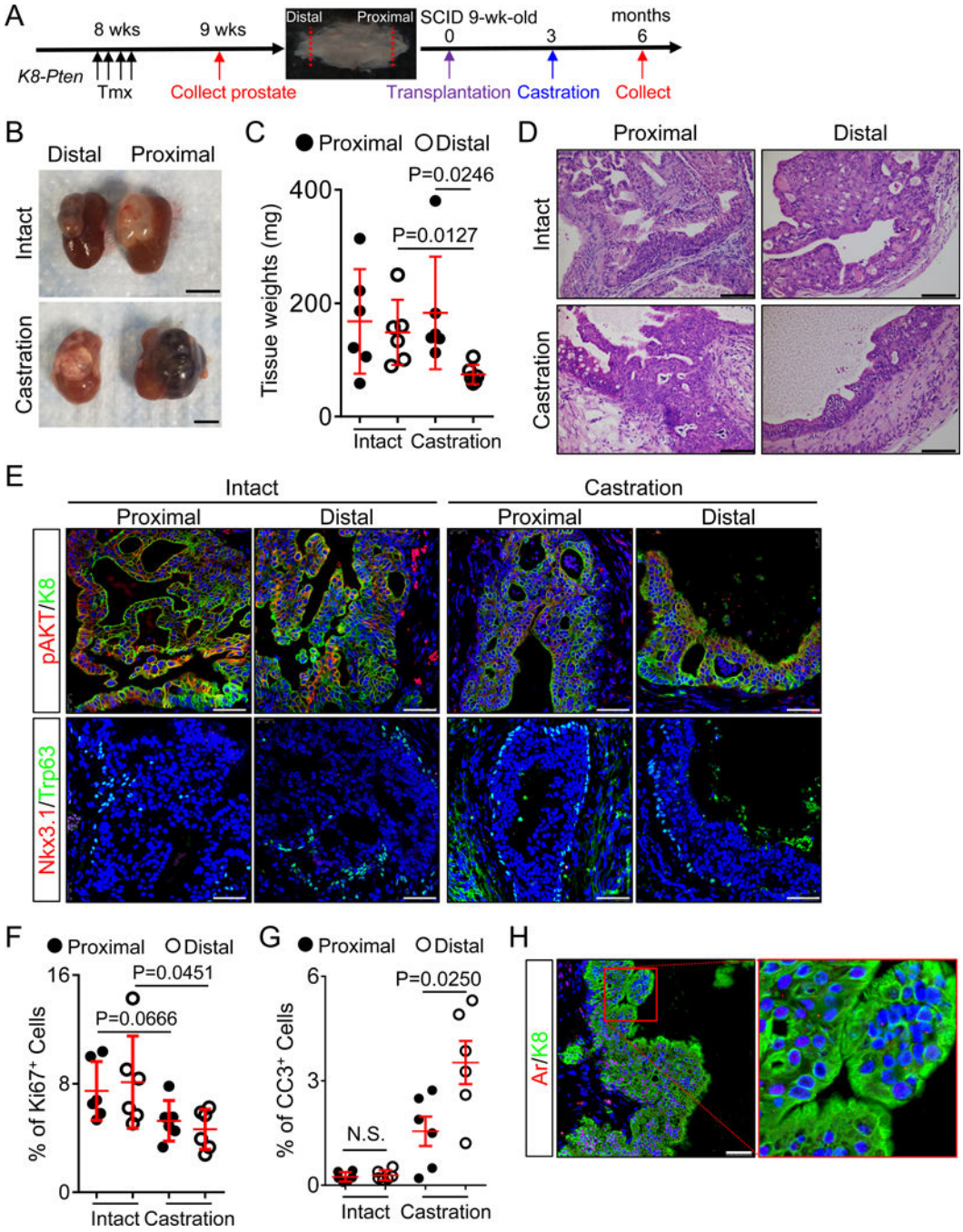

Figure 3. Transplantation experiment corroborates that prostate cancer derived from Sca-1^{+} luminal cells displays castration-resistance.

(A) Schematic illustration of experimental design. Tmx: tamoxifen. (B) Representative transillumination images of tumors outgrown from distal and proximal prostate chunks of tamoxifen-treated *K8-Pten* mice in host SCID mice underwent mock surgery and androgen deprivation-replacement. Scale bars:5 mm. (C) Dot plot shows means ± SD of weight of tumors (N=6). (D) H&E staining of transplanted tissues in intact or castrated SCID mice. Scale bars:100 μm. (E) Co-immunostaining of pAKT/K8 (upper) and Nkx3.1/Trp63 (lower) of transplants outgrown from proximal and distal prostate of tamoxifen-treated *K8-Pten*

mice in intact and castrated SCID hosts. Scale bars:50 μm. (F) Dot plot shows means ± SD of percentage of $Ki67^+$ cells (N=6, each dot shows average value from 6 representative images from each mouse). (G) Dot plot shows means ± SD of percentage of $CC3^+$ cells (N=6, each dot shows average value from 6 representative images from each mouse). (H) Co-immunostaining of Ar/K8 of transplants outgrown from proximal prostate tissues of tamoxifen-treated *K8-Pten* mice in intact SCID hosts. Scale bar: 50 μm.

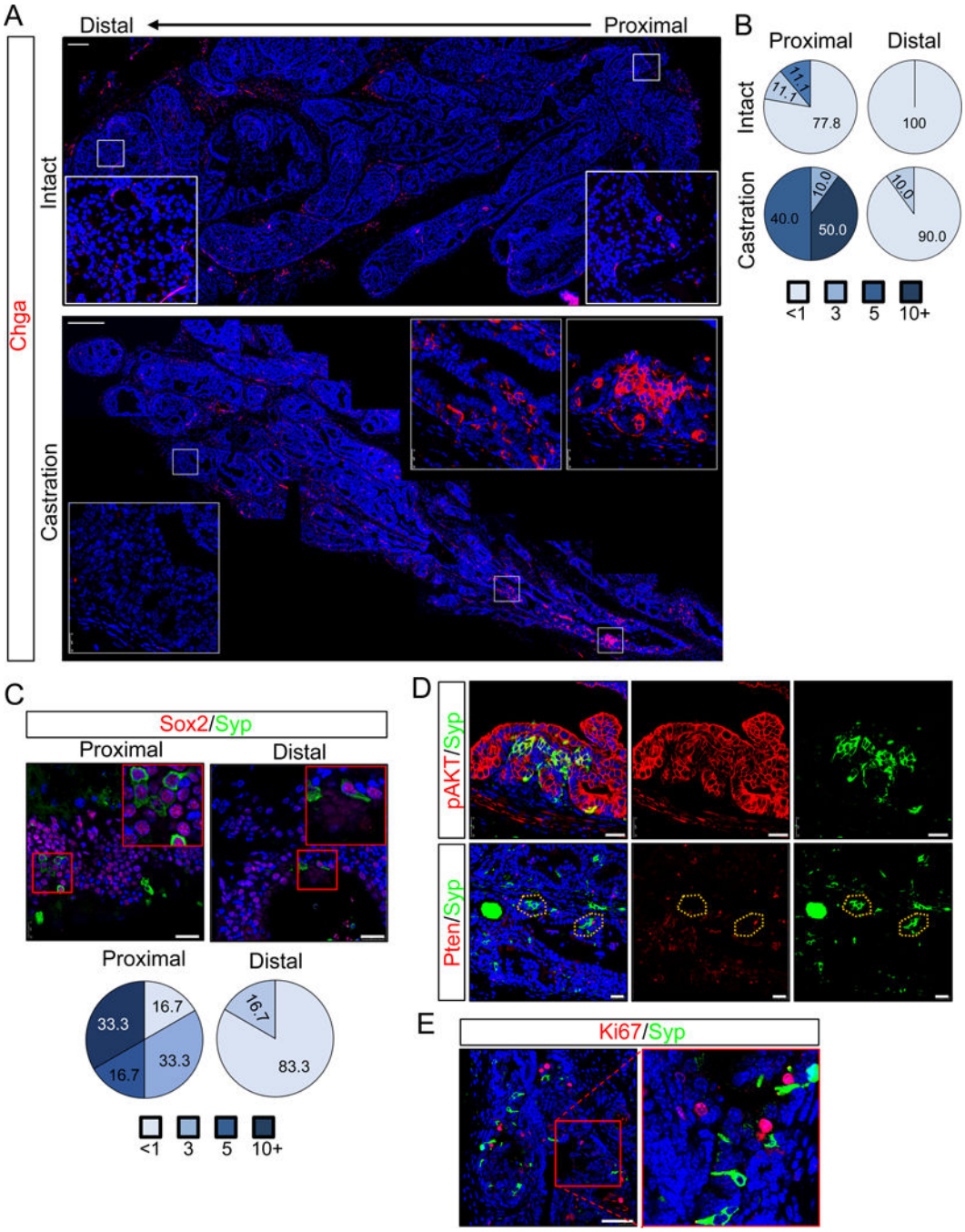

Figure 4. Androgen deprivation drives neuroendocrine differentiation of prostate cancer cells at proximal ducts of *K8-Pten* mice.

(A) Immunostaining of Chga in anterior prostates of *K8-Pten* mice at 3 months after mock surgery (intact, upper panel) or castration (castration, lower panel) and 6 months after tamoxifen treatment. Scale bar:200 μm. (B) Pie charts show quantification of size of NE colonies ($Chga^+$ or Syp^+) in proximal and distal regions of intact (N=9) and castrated (N=10) *K8-Pten* mice (results summarized from 10–20 representative images per mouse). (C) Co-immunostaining of Sox2/Syp of tumors outgrown from transplanted proximal and distal prostate of tamoxifen-treated K8-Pten mice under kidney capsules of castrated SCID

mice. Scale bars:25 μm. Pie charts show quantification of size of NE colonies ($Chga^+$ or Syp^+) (N=6, results summarized from 16–30 representative images per mouse). (D) Co-immunostaining of pAKT/Syp (upper) and Pten/Syp (lower) of proximal prostates of castrated *K8-Pten* mice. Scale bars:25 μm. (E) Co-immunostaining of Ki67/Syp in proximal prostates of castrated *K8-Pten* mice. Scale bar: 50 μm.

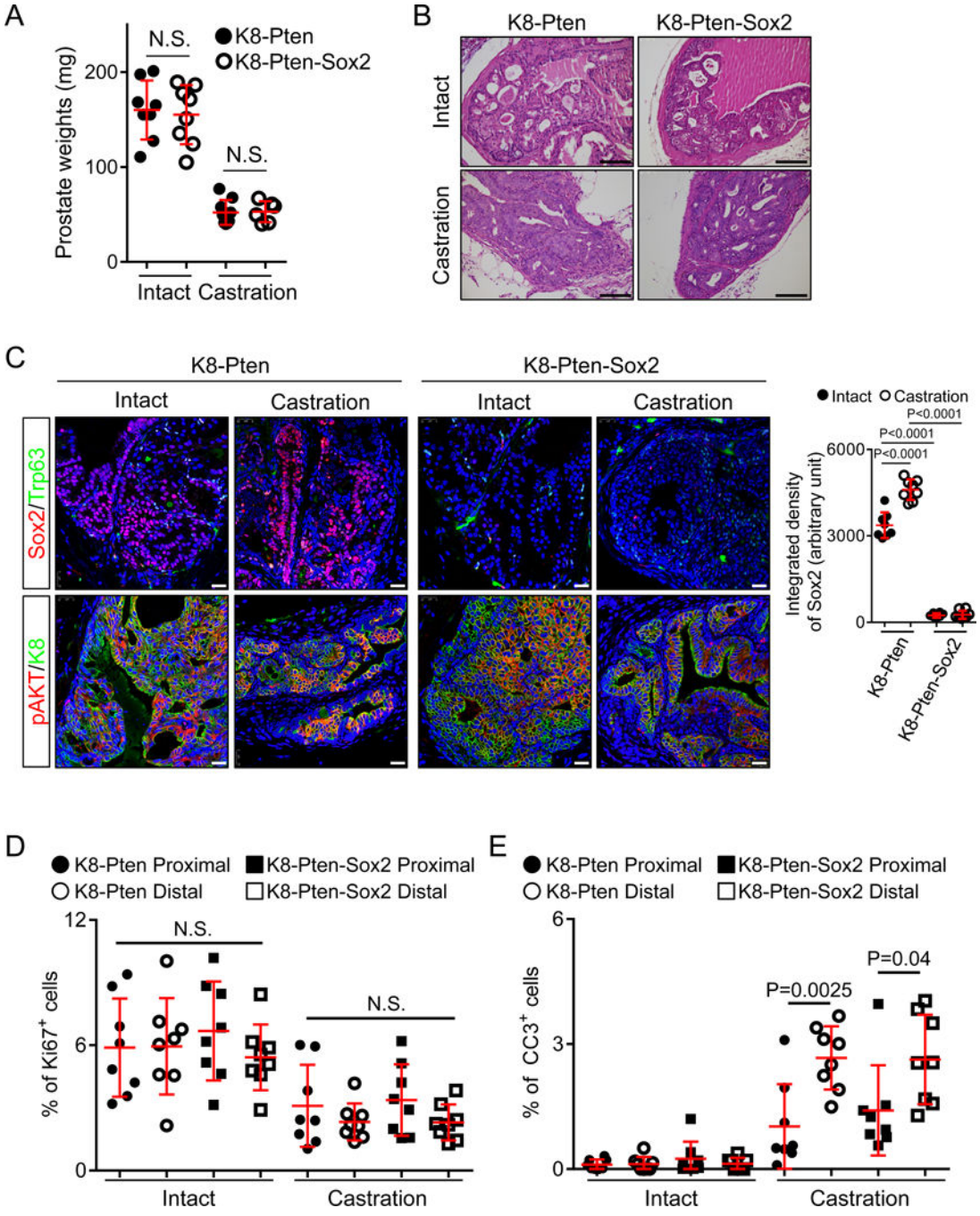

Figure 5. Sox2 is not essential for the castration resistant property.

(A) Dot plot shows means ± SD of prostate weight of intact and castrated *K8-Pten* and *K8-Pten-Sox2* mice (N=8). N.S.: no significance. (B-C) H&E staining (B) and co-immunostaining of Sox2/Trp63 (C, upper panels) and pAKT/K8 (C, lower panels) in intact and castrated *K8-Pten* and *K8-Pten-Sox2* mice. Black bars:100 μm; white bars:25 μm. Dot plot shows the integrated density of Sox2 staining (N=8, each dot represents average value from 3 representative images from each mouse). (D-E) Dot plots show means ± SD of percentages of $Ki67^+$ (D) and $CC3^+$ (E) cells in proximal and distal regions of intact and

castrated *K8-Pten* and *K8-Pten-Sox2* mice (N=8, each dot indicates average value from 6 representative images per individual mouse). N.S.: no significance.

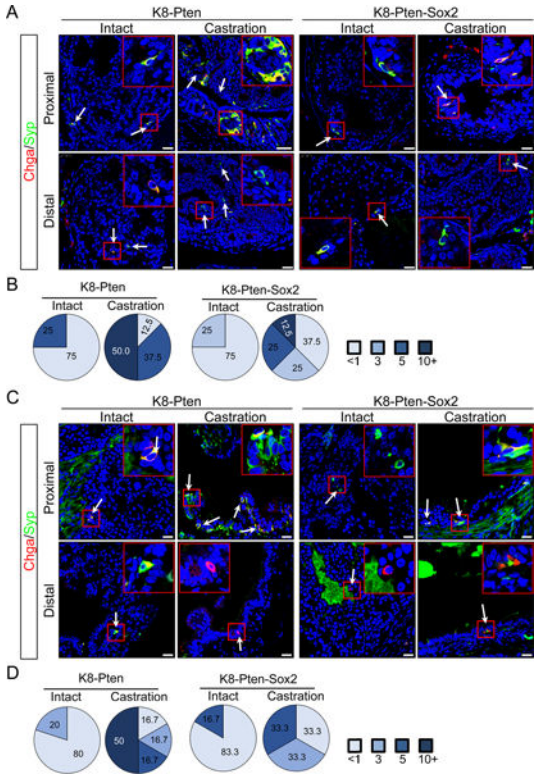

Figure 6. Sox2 is necessary for androgen deprivation-induced neuroendocrine differentiation of Pten-null prostate tumor cells.

(A) Co-immunostaining of Chga/Syp in proximal and distal prostates of intact and castrated *K8-Pten* and *K8-Pten-Sox2* mice. White arrows point to $Chga^{+}/Syp^{+}$ cells. Scale bars:25 μm. (B) Pie charts show quantification of size of neuroendocrine colony in proximal prostates of intact and castrated *K8-Pten* and *K8-Pten-Sox2* mice (N=8, results summarized from 8–15 representative images per mouse). (C) Co-immunostaining of Chga/Syp of transplanted tissues in intact and castrated SCID mice. Arrows point to neuroendocrine cells. Scale bars=25 μm. (D) Pie charts show quantification of neuroendocrine colony size. N=5–7. Results summarized from 13–25 representative images per mouse.